



Cite this: *Nanoscale*, 2015, 7, 18716

Thermal conductivity of a two-dimensional phosphorene sheet: a comparative study with graphene

Yang Hong,^a Jingchao Zhang,^{*b} Xiaopeng Huang^c and Xiao Cheng Zeng^{*a}

A recently discovered two-dimensional (2D) layered material phosphorene has attracted considerable interest as a promising p-type semiconducting material. In this work, thermal conductivity (κ) of mono-layer phosphorene is calculated using large-scale classical non-equilibrium molecular dynamics (NEMD) simulations. The predicted thermal conductivities for infinite length armchair and zigzag phosphorene sheets are $63.6^{+3.9}_{-3.9}$ and $110.7^{+1.75}_{-1.75}$ W m⁻¹ K⁻¹ respectively. The strong anisotropic thermal transport is attributed to the distinct atomic structures at altered chiral directions and direction-dependent group velocities. Thermal conductivities of 2D graphene sheets with the same dimensions are also computed for comparison. The extrapolated κ of the 2D graphene sheet are $1008.5^{+37.6}_{-37.6}$ and $1086.9^{+59.1}_{-59.1}$ W m⁻¹ K⁻¹ in the armchair and zigzag directions, respectively, which are an order of magnitude higher than those of phosphorene. The overall and decomposed phonon density of states (PDOS) are calculated in both structures to elucidate their thermal conductivity differences. In comparison with graphene, the vibrational frequencies that can be excited in phosphorene are severely limited. The temperature effect on the thermal conductivity of phosphorene and graphene sheets is investigated, which reveals a monotonic decreasing trend for both structures.

Received 31st May 2015,
Accepted 18th October 2015

DOI: 10.1039/c5nr03577e

www.rsc.org/nanoscale

1. Introduction

Phosphorene, a two dimensional counterpart of black phosphorus arranged in stacked honeycomb lattices, has attracted growing attention owing to its novel structural and electronic properties, *e.g.*, layer-dependent direct bandgaps and high electron/hole mobility.^{1–3} Through a mechanical cleavage method, phosphorene has been successfully isolated from crystalline black phosphorus.^{4–6} Phosphorene-based field-effect transistors exhibit high carrier mobility and extraordinary on/off ratios, which suggest their potential applications in nano-electronic devices. Graphene, another 2D monolayer structure, is a single layer of carbon atoms densely packed in sp² bonded honeycomb lattices. The strong and anisotropic sp² bonding and low mass carbon atoms in the microscopic structure give graphene exceptional physical and chemical characteristics compared with traditional carbon- and silicon-based materials. These extraordinary properties, *e.g.*, well

deformation beyond the linear regime,⁷ superconductivity with proper gate voltage,⁸ ballistic electronic propagation,⁹ realization of the Klein paradox,¹⁰ metal free magnetism,¹¹ *etc.*, have made graphene a promising candidate for the next generation nano-electronics.

Thermal transport in graphene and graphene-based materials has been extensively investigated by both experimental and numerical studies.^{12–15} And recently, various numerical approaches have been applied to calculate the thermal conductivity in phosphorene. By combining the density functional calculations and Peierls–Boltzmann transport equation (PBTE), Zhu *et al.*¹⁶ discovered a peculiar coexistence phenomenon of size-dependent and size-independent thermal conductivities in phosphorene. The computed κ of armchair and zigzag phosphorenes are 24.3 and 83.5 W m⁻¹ K⁻¹ respectively. The anisotropy in thermal conductivity is attributed to the orientation dependent group velocities and relaxation times. A significant crystallographic orientation dependence of thermal conductance is observed using first-principles calculations combined with the non-equilibrium Green's function method.¹⁷ It is found that the zigzag-oriented thermal conductance is enhanced when a zigzag-oriented strain is applied but decreases when an armchair oriented strain is applied; whereas the armchair-oriented thermal

^aDepartment of Chemistry, University of Nebraska-Lincoln, Lincoln, NE 68588, USA

^bHolland Computing Center, University of Nebraska-Lincoln, Lincoln, NE, 68588, USA. E-mail: zhang@unl.edu, xzeng1@unl.edu

^cDepartment of Mechanical Engineering, Massachusetts Institute of Technology, Cambridge, Massachusetts 02139, USA

conductance always decreases when either a zigzag or an armchair oriented strain is applied. In another first-principles calculations, κ of phosphorenes are predicted as 36 and 110 $\text{W m}^{-1} \text{K}^{-1}$ at 300 K along its armchair and zigzag directions respectively.¹⁸ By solving the phonon Boltzmann transport equation (BTE) based on first-principles calculations, Qin *et al.*¹⁹ computed the κ of phosphorene as 13.65 $\text{W m}^{-1} \text{K}^{-1}$ (armchair) and 30.15 $\text{W m}^{-1} \text{K}^{-1}$ (zigzag) at 300 K, showing an appreciable anisotropy along different directions.

Despite the successful application of first-principles approaches on predicting the thermal conductivity of phosphorene, its modeling ability is highly restricted by its spatio-temporal scales and demanding computational costs. Classical molecular dynamics (MD), in which the system is driven by the quantum mechanics derived interatomic energy potential, provides a reasonable balance between modeling accuracy, size scale, and speed. In this work, thermal conductivities of the 2D phosphorene sheet in the armchair and zigzag directions are computed using large-scale classical MD simulation. Various phosphorene structures with lengths up to 500 nm are constructed. Periodic boundary conditions are applied in the width direction of all cases to eliminate the size effect. A non-equilibrium molecular dynamics approach is used for the thermal conductivity characterization. As a comparative study, κ of graphene in the armchair and zigzag directions with equivalent dimensions is computed. Detailed phonon density of states analyses are performed to help explain the thermal conductivity differences between phosphorene and graphene. Temperature dependence of thermal conductivity is explored from 100 to 400 K.

2. Models, physical basis, and computational approach

All MD simulations in this work are performed using the open-source classical molecular dynamics code and large-scale atomic/molecular massively parallel simulator (LAMMPS).²⁰ A Stillinger–Weber (SW) potential is parametrized by Jiang *et al.*²¹ to describe the P–P interactions in monolayer black phosphorus. An important cross-pucker interaction (CPI), which describes the interaction strength between two neighboring puckers, is introduced to fully describe the buckled structure in the phosphorene sheet. The calculated phonon dispersions of the phosphorene sheet using this SW potential agree well with the first-principles results.²² In the following work, the SW parameters are further optimized and adapted in the LAMMPS using the valence force field (VFF) model.²³ The bond stretching, intra-group angle bending and inter-group angle bending are all described by the SW potential and optimized in the parameterization process. The anharmonic portion in the SW potential has provided reasonably accurate information for nonlinear effects in covalent systems.²⁴ This nonlinear property is important for MD simulations of nonlinear phenomena like thermal conductivity. The nonlinear

effects through the nonlinear forms of both two-body and three-body terms are included in the SW potential. Moreover, since phonons are the most important heat energy carrier in the thermal transport in monolayer phosphorene, the phonon spectrum plays a crucial role in the thermal conductivity. The acoustic phonon velocities from the phonon spectrum are closely related to the mechanical properties of the material.²⁵ As a result, a good fitting to the phonon spectrum will usually lead to a good description for mechanical properties. In this work, the VFF-based SW potential is used to describe the phosphorene system.²³ Atomic configurations of phosphorene are depicted in Fig. 1. Periodic boundary conditions are applied in the width direction. To examine the effect of the size perpendicular to the heat flux direction, we varied the domain width from 5.1 to 20.4 nm. Similar thermal conductivities were obtained from the simulations with different widths. As a result, a moderate width of ~ 10 nm is chosen for all simulations to reduce the computational cost. In the SW potential, the top and bottom P atoms are treated as two atomic types. Thermal conductivities along the zigzag (x) and armchair (y) directions are calculated respectively in this work. The initial buckling distance is set as 2.13 Å. For graphene modeling, the second generation of the Brenner potential,²⁶ the reactive empirical bond-order (REBO) potential based on

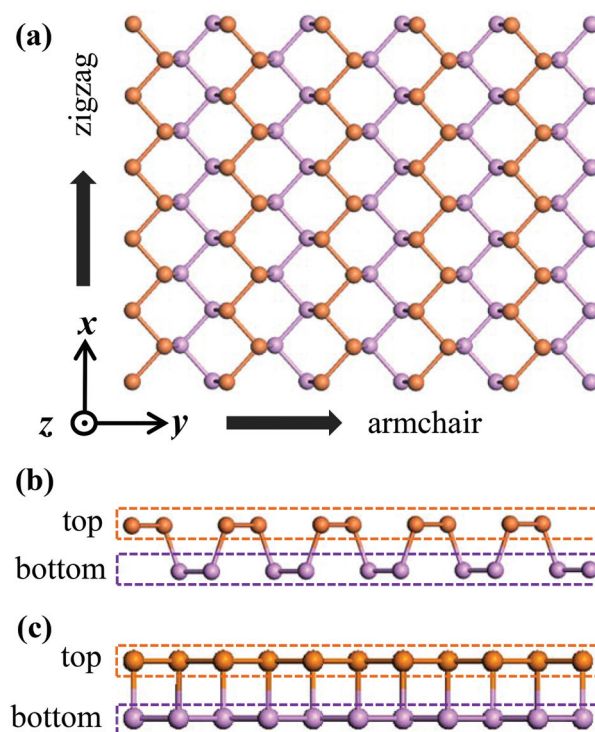


Fig. 1 (a) Top view of the monolayer phosphorene structure. Zigzag boundary is along the x direction and armchair is along the y direction. (b) Front view of phosphorene from the x direction. The top and bottom P atoms are grouped as two atomic types for accurate inter/intra-layer interaction descriptions. (c) Side view of phosphorene from the y direction.

the Tersoff potential^{27,28} with interactions between C–C bonds, is employed. The REBO potential is chosen because its functions and parameters are known to give reasonable predictions for the thermal properties of graphene, whereas the adaptive intermolecular reactive empirical bond order (AIREBO) was reported to underestimate the dispersion of ZA (out-of-plane acoustic) phonons in graphene.²⁹ The integration time step is 0.5 fs (1 fs = 10⁻¹⁵ s) for all simulations in this work.

The thermal conductivities of 2D phosphorene and graphene sheets are calculated using a non-equilibrium molecular dynamics approach. In a way similar to experiments, a temperature gradient can be applied with the use of heat reservoirs to evaluate the resulting heat flux. The thermal energies will flow until equilibration is established in the heat-flux direction. This transport phenomenon derived from the non-equilibrium state provides the basis of direct non-equilibrium molecular dynamics (dNEMD) simulations. The thermal conductivity is then obtained using the Fourier's law of heat conduction;

$$J = -\kappa A \partial T / \partial x \quad (1)$$

where A is the cross-sectional area and x represents the heat flux direction. In this work, thermal conductivities along both the x and y axes are calculated. The parameter x denoted in eqn (1) represents the direction of interest. Alternatively, the need of external thermostating can be suppressed by swapping the cause and the effect. In reverse-NEMD (rNEMD) simulations, a heat flux is imposed by regularly adding/subtracting the kinetic energies to/from hot and cold particles resulting in a temperature profile that can be determined once the steady state is reached.³⁰ In this way, the total energy and total linear momentum are conserved; hence no external thermostating is needed. In this work, the latter approach is applied. After the MD system reaches thermal equilibrium, four layers of atoms at each end are grouped to add and subtract thermal energies respectively by scaling the velocity of each atom by the same factor χ . Heat bath and heat sink are created by adding kinetic energy ΔE_k in the hot region and removing the same amount from the cold one while preserving linear momentum at each time step. As time goes on, a constant heat flux (J) from the hot to the cold region will be established. Atoms along the heat flux direction are grouped into equal thickness slabs with more than 30 atoms per section. The temperature values (T) in each slab are recorded after the temperature distribution reaches the steady state. The thermal conductivity of the 2D sheet is evaluated from the Fourier's law. In previous experimental studies of graphene's thermal conductivity, Balandin *et al.*^{31,32} used the value of 0.35 ± 0.01 nm as the thickness of single layer graphene. Most of the numerical work studying the thermal conductivity of graphene chose the value of 3.35 Å as the thickness.^{33–37} Therefore, our calculation of graphene's thermal conductivity uses the same thickness value (3.35 Å) as used in most of the experimental and numerical studies. This provides a common base when comparing our results with those by other researchers. The thickness of phosphorene is

chosen as the bulk layer separation distance 5.25 Å, which is around the same value as used in previous studies.^{18,19,38,39} Since the calculated thermal conductivity scales linearly with layer thickness, our results can be adjusted easily for other options.

During NEMD simulations, it is important to verify that the temperature gradient along the heat flux direction has reached the steady state before data collection. At thermal equilibrium, the atomic velocity distribution should follow the Maxwellian distribution;

$$P_M = 4\pi v^2 \left(\frac{m}{2\pi k_B T} \right)^{3/2} e^{-mv^2/2k_B T} \quad (2)$$

where P_M is the probability of an atom moving with a velocity v , m represents the atom mass, and k_B is the Boltzmann constant. The velocity distribution based on the simulation results and the Maxwellian distribution are compared to verify that the temperature gradient has reached the steady state. In MD simulations, the temperature of the system is calculated by the energy equipartition theorem,

$$\langle E \rangle = \sum_1^N \frac{1}{2} m v_i^2 = \frac{3}{2} N k_B T_{MD} \quad (3)$$

where v_i is the velocity of atom i . Since quantum effects are not considered in classical MD simulations, eqn (3) is only valid at high temperatures. The Debye temperatures (T_D) of graphene (2300 K and 1287 K respectively for in-plane and out-of-plane phonons) are much higher than the MD temperatures 100–400 K used in this work. Therefore quantum corrections are applied to the calculated temperatures before performing graphene's thermal conductivity calculations. The quantum correction equation for the 2D graphene model is expressed as

$$T_{MD} = \frac{2}{3} T_{LA} x_{LA}^{-3} \int_0^{x_{LA}} \frac{x^2}{e^x - 1} dx + \frac{2}{3} T_{TA} x_{TA}^{-3} \int_0^{x_{TA}} \frac{x^2}{e^x - 1} dx + \frac{1}{3} T_{ZA} x_{ZA}^{-3} \int_0^{x_{ZA}} \frac{x}{e^x - 1} dx \quad (4)$$

where T_{MD} is the temperature in the MD simulation; T_{LA} , T_{TA} , and T_{ZA} are the Debye temperatures of three different acoustic modes in graphene, which are 2840, 1775, and 1120 K respectively; and x_{LA} , x_{TA} , and x_{ZA} are the ratios of corrected temperatures (temperatures after quantum correction, denoted as T) and Debye temperatures. A previous study by Zhang *et al.*³⁵ proved that eqn (4) can accurately predict the specific heat of graphene at $T_{MD} = 300$ K. MD temperatures of 275 K and 325 K correspond to 658.8 K and 725.8 K separately after quantum correction, indicating its importance in graphene's thermal conductivity calculations. The Debye temperature of phosphorene is reported as ~280 K–500 K,^{18,19,40} which is comparable to the temperature range used in this study. Thus no quantum corrections are applied to the temperatures of the phosphorene sheet in its thermal conductivity calculations.

To help analyze the thermal conductivity results of phosphorene and graphene sheets, phonon density of states

(PDOS) is calculated by taking the Fourier transform of the velocity autocorrelation function (VACF)

$$F(\omega) = \frac{1}{\sqrt{2\pi}} \int_{-\infty}^{\infty} dt e^{i\omega t} \frac{\langle v(0)v(t) \rangle}{\langle v(0)v(0) \rangle} \quad (5)$$

Higher values of PDOS for a phonon with frequency ω means more states are occupied by it. And zero PDOS means that no phonon with frequency ω exists in the system. The phonon power spectrum analysis provides a quantitative means to assess the power carried by different phonon modes in a system. Due to the decoupled nature between the in-plane and out-of-plane phonons in graphene,^{41–43} the decomposed PDOS in each direction is calculated for both graphene and phosphorene sheets as a comparison.

3. Results and discussion

Fig. 2(a) illustrates the NEMD setup in the $9.9 \times 40.2 \text{ nm}^2$ ($x \times y$) phosphorene for heat conduction in the armchair direction. Periodic boundary conditions are applied in the width (x) direction to eliminate the size effect. Free boundaries are used in the heat flux y direction and out-of-plane z direction. The outmost layers of P atoms denoted in black are fixed. For thermal equilibrium calculations, 500 ps ($1 \text{ ps} = 10^{-12} \text{ s}$) canonical ensemble (NVT) and 500 ps micro-canonical ensemble (NVE) calculations are performed on the phosphor-

ene system successively. After the system reaches thermal equilibrium at a given temperature of 300 K, four layers of atoms are grouped at each end to create the heat bath and heat sink respectively. Thermal energy $Q_{\text{in}} = 3.23 \times 10^{-8} \text{ W}$ is added to the heat bath at each time step and the same amount Q_{out} is subtracted from the heat sink constantly for another 4 ns ($1 \text{ ns} = 10^{-9} \text{ s}$). Since the total energy in the system is constant during the heating/cooling process, the overall temperature remains unchanged. Temperature distribution along the heat flux direction at a steady state is shown in Fig. 2(b). The atomic configuration of the phosphorene system after the heating/cooling process is shown in the inset. Linear fitting is applied to the calculated temperature gradient and thermal conductivity is calculated using eqn (1). During the NEMD process, kinetic energies are constantly added/subtracted in the heating/cooling areas for temperature control. In this ultrafast energy exchange process, kinetic energy and potential energy within the heating/cooling regions are in a non-equilibrium state and phonon boundary scattering is extremely rapid at the interface. Therefore the temperature drop is non-linear in these regions and should be eliminated from the thermal conductivity calculations.^{44–47} The calculated thermal conductivity of the [$9.9 \times 40.2 \text{ nm}^2$] phosphorene in the armchair direction is $3.9 \text{ W m}^{-1} \text{ K}^{-1}$ and κ of similar sized [$39.9 \times 10.0 \text{ nm}^2$] phosphorene in the zigzag direction is $11.7 \text{ W m}^{-1} \text{ K}^{-1}$. The thermal conductivity anisotropy can be quantified by the ratio (χ) of maximum and minimum direction-dependent thermal conductivities. A factor of $\chi = 3$ anisotropy is attained from the above results, the same as shown in previous calculations.¹⁸ As a comparative study, thermal conductivities of graphene in the armchair direction and zigzag direction of similar dimensions are calculated, which are $209.3 \text{ W m}^{-1} \text{ K}^{-1}$ and $213.6 \text{ W m}^{-1} \text{ K}^{-1}$, respectively. The simulation setup and data processing procedures of graphene's κ calculation are the same as those of the phosphorene sheet, except for the extra quantum correction process as stated in the previous section.

To assure that the temperature distribution in the 2D sheet has reached the steady state before and after the heating/cooling process, atom velocities are extracted from the MD system and compared with Maxwellian velocity distribution at the same temperature. Taking the [$9.94 \times 40.19 \text{ nm}^2$] phosphorene for heat conduction in the armchair direction as an example, after successive NVT and NVE simulations, a snapshot of the atom velocities is taken. The statistical velocity distribution is mapped across the range from 0 to 1400 m s^{-1} , as is shown in Fig. 3(a). Another snapshot is taken after the 4 ns heating/cooling process is completed. Fig. 3(b) shows that the temperature gradient along the heat flux direction is constant before data collection. An alternative way to prove that the system has reached the steady state is to record the temperature differences between the heating and cooling regions. Since the latter requires a relatively large temperature bias to suppress the data noise, the former approach is used in this work.

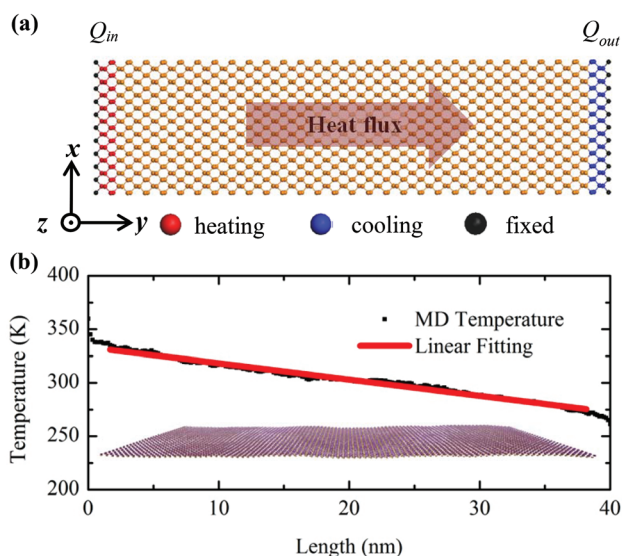


Fig. 2 (a) Illustration of the NEMD process. Black atoms at the boundaries of the system are fixed in the position. Free boundary is used in the out-of-plane z direction. Periodic boundary conditions are applied in the width (x) direction. Red and blue areas are denoted as heat bath and heat sink respectively. (b) Temperature distribution along the heat flux direction (y) in the $9.94 \times 40.19 \text{ nm}^2$ ($x \times y$) phosphorene in the armchair direction. The red solid line denotes the linear fitting results. The atomic configuration of phosphorene after the heating/cooling process is shown in the inset.

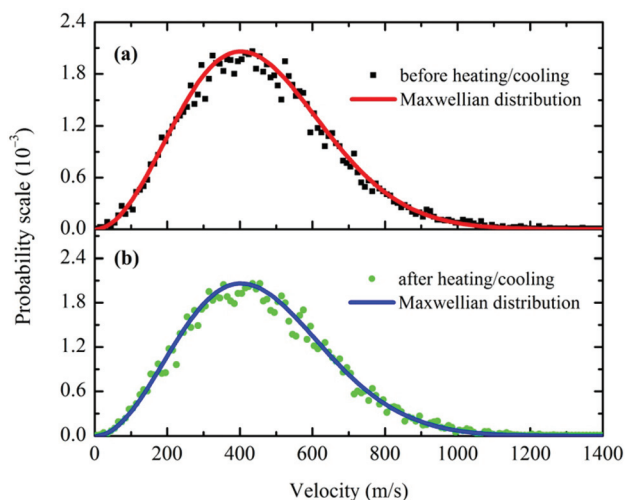


Fig. 3 Atomic velocity distributions in $9.94 \times 40.19 \text{ nm}^2$ ($x \times y$) armchair phosphorene. (a) Velocity distribution after 500 ps NVT and 500 ps NVE simulations. (b) Velocity distribution after 4 ns NEMD simulations. A good agreement between the MD simulation and Maxwellian velocity distribution is observed, indicating that the temperature distribution has reached the steady state before data collection.

Length dependence of thermal conductivities of the phosphorene sheet in the armchair and zigzag directions and the graphene sheet in the armchair and zigzag directions are presented in Fig. 4(a). Lengths of 10, 20, 40, 80, 120, 160, 300, 400 and 500 nm are simulated. Widths of all 2D systems have the same value of $\sim 10.0 \text{ nm}$ with periodic boundary conditions. Fig. 4(a) shows that the thermal conductivities of the phosphorene sheet are around one order of magnitude lower than those of the graphene sheet. The computed thermal conductivity of phosphorene in the armchair direction ranges from 2.0 to $21.7 \text{ W m}^{-1} \text{ K}^{-1}$, and 6.2 – $73.6 \text{ W m}^{-1} \text{ K}^{-1}$ in the zigzag direction. On the other hand, the calculated κ results of graphene in the armchair and zigzag directions range from 73.0 to $657.6 \text{ W m}^{-1} \text{ K}^{-1}$ and 75.0 to $690.6 \text{ W m}^{-1} \text{ K}^{-1}$, respectively. The measured thermal conductivity of graphene from the experiments is around 3000 – $5000 \text{ W m}^{-1} \text{ K}^{-1}$ for a sample length of $\sim 10 \mu\text{m}$.^{48,49} This high thermal conductivity exceeds that of graphite and is partly attributed to the long phonon mean free path (MFP). Numerical simulations have reported much smaller κ values of graphene due to the confined system sizes and stronger phonon boundary scattering.^{50,51} The calculation results in Fig. 4(a) indicate that the anisotropic thermal transport in the phosphorene sheet is much more significant than that in the graphene sheet. This high anisotropy is partially attributed to the direction-dependent group velocities and anisotropic phonon dispersion in phosphorene.¹⁸ A maximum factor of $\chi = 4.9$ anisotropy is observed in the 300 nm long phosphorene sheet. It is speculated that the distinct pucker structures in the armchair and zigzag directions also contribute to the strong anisotropic thermal conductivities in the phosphorene sheet. As is shown in Fig. 1(b), the

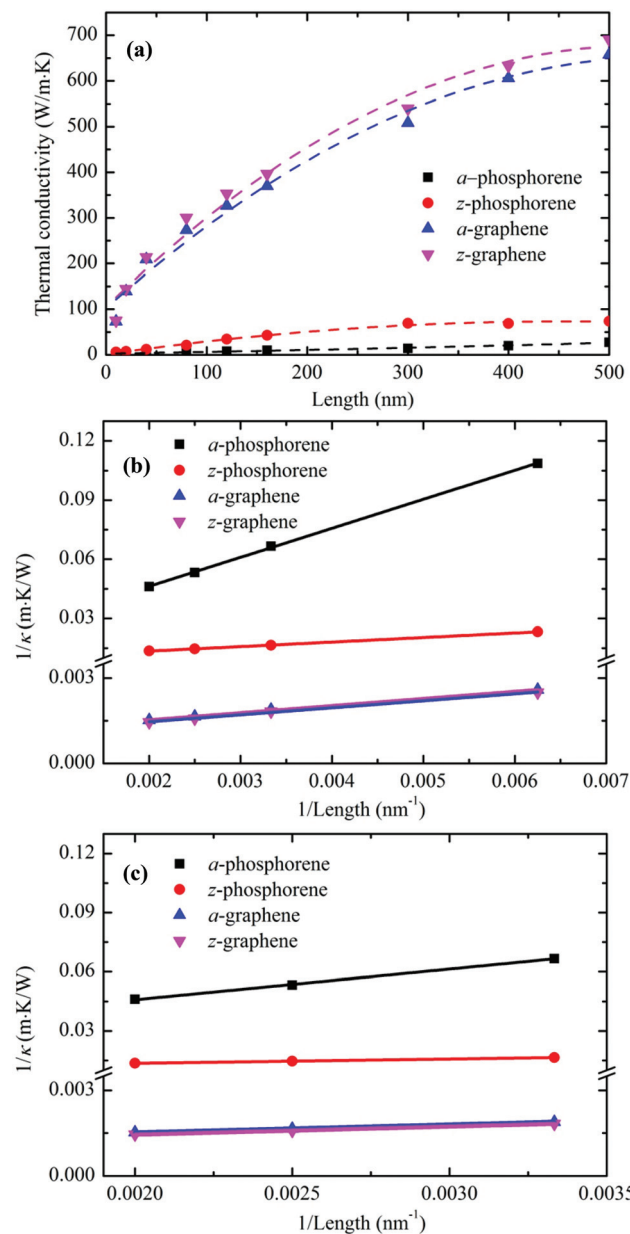


Fig. 4 (a) Thermal conductivities of phosphorene and graphene in the armchair or zigzag directions versus length. Second order polynomial fittings (dashed lines) are applied to the data sets to guide the eye. (b) and (c) The corresponding linear relationship between $1/\kappa$ and $1/L$ of 160–500 nm and 300–500 nm phosphorene sheets. a and z stand for the armchair and zigzag directions, respectively.

top and bottom P layers in phosphorene extend alternatively in the armchair direction, while in the zigzag direction shown in Fig. 1(c), the top and bottom P atoms are superposed in the out-of-plane direction continuously. On the other hand, the anisotropic thermal transport in graphene is attributed to two major factors: (1) different phonon boundary scattering along the altered chiral directions; and (2) strong localization of phonons in regions near and at the edges of graphenes,

especially graphenes in the armchair direction, which suppresses thermal transport.^{52–54}

The calculated thermal conductivity results are fitted using a linear function for lengths of 160–500 nm,⁵⁵

$$\frac{1}{\kappa} = \frac{1}{\kappa_{\infty}} \left(\frac{l}{L} + 1 \right) \quad (6)$$

where l is the effective phonon MFP and κ_{∞} is thermal conductivity of the 2D sheet. The fitting results using 160, 300, 400 and 500 nm points for $1/\kappa$ and $1/L$ are shown in Fig. 4(b). It has been suggested that eqn (6) is valid only when the system size is comparable or larger than the phonon MFP that dominates thermal transport.⁵⁶ Qin *et al.*¹⁹ calculated the representative MFP of armchair and zigzag phosphorene at 83 nm and 66 nm correspondingly. For confined graphene systems used in MD simulations, the effective phonon MFP ranges from 80 to 240 nm.^{57,58} Therefore, the system sizes used in the linear extrapolation fulfill the linear fitting requirement. The predicted thermal conductivities of infinite length phosphorene sheets in the armchair and zigzag directions are 59.7 and 112.4 W m⁻¹ K⁻¹ respectively, which are on the same order of magnitude with the first-principles predictions.¹⁸ To test the convergence of the predicted κ results, extrapolations using only 300, 400 and 500 nm lengths are also performed. The calculated κ results of the phosphorene sheet in the armchair and zigzag directions are 67.5 and 108.9 W m⁻¹ K⁻¹. The fitting results using only 300, 400 and 500 nm points are shown in Fig. 4(c). The averaged thermal conductivity results of the phosphorene sheets can be presented as 63.6^{+3.9}_{-3.9} and 110.7^{+1.75}_{-1.75} W m⁻¹ K⁻¹, in the armchair and zigzag directions, respectively. Similarly, the extrapolated κ for graphene sheets using four data points are 970.9 and 1027.8 W m⁻¹ K⁻¹, in the armchair and zigzag directions, respectively, and 1046.0 and 1145.9 W m⁻¹ K⁻¹ using only three data points. The averaged results are expressed as 1008.5^{+37.6}_{-37.6} and 1086.9^{+59.1}_{-59.1} W m⁻¹ K⁻¹ for graphene sheets in the armchair and zigzag directions, respectively. The result deviations range from 1% to 6% for all cases, which can be considered as good convergence for the predicted κ values of both phosphorene and graphene sheets. To gain further insight into the thermal conductivity differences between phosphorene and graphene, PDOS are calculated for phosphorene and graphene sheets with dimensions of 10 × 40 nm². Due to the decoupled nature between the in-plane and out-of-plane phonons in graphene, decomposed PDOS in x , y and z directions are calculated separately for both structures. The calculated results are shown in Fig. 5(a)–(d). The reported PDOS of the graphene sheet soundly matches previous MD simulation results,^{59–62} which illustrates that the flexural branch (ZA) dominates the low frequency acoustic phonons while the in-plane longitudinal (LA) and transverse (TA) branches occupy the high frequency phonons. Compared with graphene, it is clear that the vibrational frequencies that can be excited in phosphorene

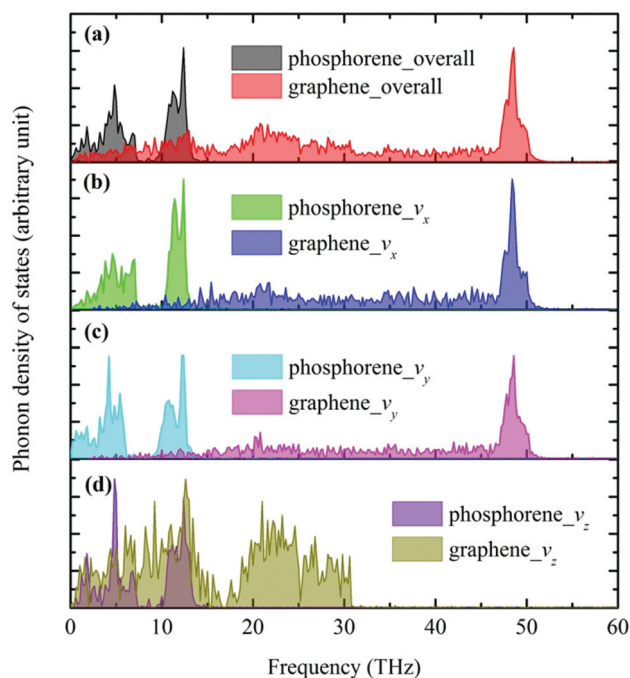


Fig. 5 (a) PDOS of phosphorene and graphene sheets (for heat conduction in the armchair direction), respectively, at temperature 300 K. (b–d) Decomposed PDOS in x , y and z directions. The PDOS peak locations remain unchanged in the phosphorene sheet, while the in-plane and out-of-plane phonons of the graphene sheet are anisotropic.

are severely limited. The active phonon frequencies of the phosphorene sheet ranges from 0 to 15 THz, while in graphene, the lateral phonons dominate the high frequencies up to 52 THz and flexural phonon occupies the low frequency acoustical branches. The observed remarkable differences in PDOS could account for the vast disparity in the thermal conductivities of phosphorene and graphene sheets. Although for a long time it has been tacitly accepted that the in-plane acoustic phonons are dominant in the thermal transport of graphene,^{63–65} recent studies have shown that the fact is quite different. By measuring the thermal transport of single layer graphene (SLG) supported on amorphous SiO₂, Seol *et al.*⁶⁶ performed a revised calculation and showed that the ZA branch can contribute as much as 77% at 300 K and 86% at 100 K of the calculated thermal conductivity for the suspended graphene due to the high specific heat and long mean scattering time of ZA phonons. Based on the exact numerical solution of the linear Boltzmann transport equation (BTE), Lindsay *et al.*^{29,67} calculated the lattice thermal conductivity (κ_L) of graphene at 300 K and it turned out that the dominant contribution to κ_L comes from the ZA branch, which is greater than the combined TA and LA contributions. Unlike those of the graphene sheet, the in-plane and out-of-plane phonons of the phosphorene sheet have the same PDOS frequencies in all directions, as is shown in Fig. 5(b)–(d). The differences from the flexural phonon contributions also con-

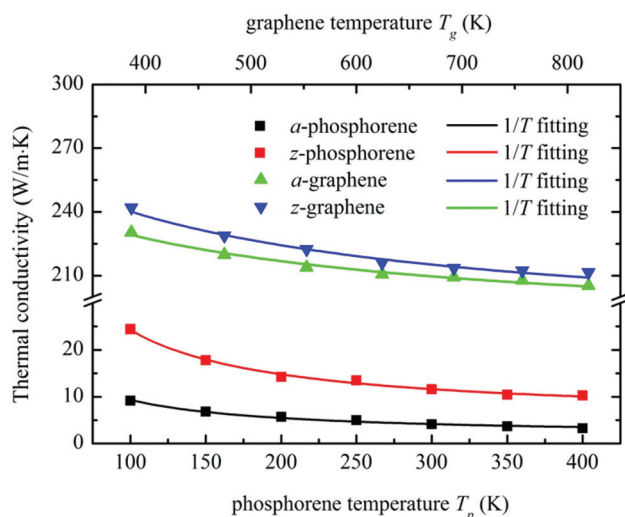


Fig. 6 Temperature dependence of thermal conductivity for phosphorene/graphene in the armchair and zigzag directions. Fitting results by the inverse relationship with temperature ($\kappa \sim 1/T$) are plotted with solid lines. Quantum correction is applied to the MD temperature of the graphene sheet and shown in the top x axis.

tribute to the different κ results in phosphorene and graphene sheets.

In practical applications, phosphorene and graphene could be placed in various working conditions at different temperatures. Therefore it is necessary to investigate the temperature dependence of their thermal conductivity. Aside from the 300 K used in previous calculations, temperatures of 100, 150, 200, 250, 350 and 400 K are applied and the calculated κ results are shown in Fig. 6. The dimensions of the phosphorene sheet in the armchair and zigzag directions are $9.94 \times 40.19 \text{ nm}^2$ and $39.93 \times 9.99 \text{ nm}^2$, respectively, and $9.84 \times 40.05 \text{ nm}^2$ and $39.98 \times 10.01 \text{ nm}^2$ for the graphene sheet in the armchair and zigzag directions, respectively. Quantum corrections are applied to the MD temperatures of graphene (T_g), as is shown in the top x axis of Fig. 6. It is observed from Fig. 6 that κ of both phosphorene and graphene sheets decreases monotonically with temperature, which is as expected for phonon dominated crystalline materials. As the system temperature increases, higher frequency phonons become activated and the phonon population grows. As a result, the Umklapp phonon scattering becomes more severe, which directly reduces the thermal conductivity in the 2D sheet. The maximum κ reduction of the phosphorene sheet in the armchair and zigzag directions, and the graphene sheet in the armchair and zigzag directions are calculated as 64%, 58%, 11%, and 13%, respectively. The calculated thermal conductivity results are fitted with an inverse relationship with temperature ($\kappa \sim 1/T$). It can be observed that the fitting curves soundly match the calculated thermal conductivities, indicating the Umklapp scattering is dominant at this temperature range.⁶⁸

4. Conclusion

Using large-scale classical MD simulations, thermal conductivities of monolayer phosphorene are computed and compared with graphene. Using a linear extrapolation method, thermal conductivities of 2D phosphorene sheets in the armchair and zigzag directions are predicted as $63.6_{-3.9}^{+3.9}$ and $110.7_{-1.75}^{+1.75} \text{ W m}^{-1} \text{ K}^{-1}$, respectively. In comparison, κ of graphene sheets are calculated to be $1008.5_{-37.6}^{+37.6}$ and $1086.9_{-59.1}^{+59.1} \text{ W m}^{-1} \text{ K}^{-1}$ in the armchair and zigzag directions, respectively. The calculated thermal conductivities of the phosphorene sheet are around one order of magnitude lower than those of the graphene sheet. On the other hand, the high scale of anisotropy exceeds that of graphene. Detailed PDOS analyses reveal that the in-plane and out-of-plane phonons in phosphorene share the same peak frequencies from 0 to 15 THz, while in graphene, the lateral phonons dominate the high frequencies up to 52 THz and flexural phonons occupy the low frequency acoustical branches. Therefore, it can be speculated that different thermal conductivities between phosphorene and graphene are mainly from two aspects: (1) severely limited vibrational frequencies in phosphorene compared with graphene; and (2) less contributions from the out-of-plane flexural phonons in phosphorene. Temperature dependence of thermal conductivity is investigated and a monotonic decreasing trend is found for both structures. Our work provides a fundamental understanding of thermal transport in phosphorene and can be considered for improving certain nano-device performances with phosphorene-based thermal interface materials.

Acknowledgements

We thank Dr Jun Dai for useful discussions. Support of this work from Nebraska Center for Energy Sciences Research and Holland Computing Center of the University of Nebraska-Lincoln is greatly appreciated.

References

- 1 J. Dai and X. C. Zeng, *RSC Adv.*, 2014, **4**, 48017–48021.
- 2 H. Guo, N. Lu, J. Dai, X. Wu and X. C. Zeng, *J. Phys. Chem. C*, 2014, **118**, 14051–14059.
- 3 J. Dai and X. C. Zeng, *J. Phys. Chem. Lett.*, 2014, **5**, 1289–1293.
- 4 L. Li, Y. Yu, G. J. Ye, Q. Ge, X. Ou, H. Wu, D. Feng, X. H. Chen and Y. Zhang, *Nat. Nanotechnol.*, 2014, **9**, 372–377.
- 5 H. Liu, A. T. Neal, Z. Zhu, Z. Luo, X. Xu, D. Tománek and P. D. Ye, *ACS Nano*, 2014, **8**, 4033–4041.
- 6 F. Xia, H. Wang and Y. Jia, *Nat. Commun.*, 2014, **5**, 4458.
- 7 C. Lee, X. Wei, J. W. Kysar and J. Hone, *Science*, 2008, **321**, 385–388.

- 8 A. Ballestar, P. Esquinazi, J. Barzola-Quiquia, S. Dusari, F. Bern, R. R. da Silva and Y. Kopelevich, *Carbon*, 2014, **72**, 312–320.
- 9 Y. P. Bliokh, V. Freilikher and F. Nori, *Phys. Rev. B: Condens. Matter*, 2013, **87**, 245134.
- 10 B. V. Duppen and F. M. Peeters, *EPL*, 2013, **102**, 27001.
- 11 V. V. Ilyasov, B. C. Meshi, V. C. Nguyen, I. V. Ershov and D. C. Nguyen, *Solid State Commun.*, 2014, **199**, 1–10.
- 12 H. Y. Li, H. Ying, X. P. Chen, D. L. Nika, A. I. Cocemasov, W. W. Cai, A. A. Balandin and S. S. Chen, *Nanoscale*, 2014, **6**, 13402–13408.
- 13 B. Mortazavi, M. Potschke and G. Cuniberti, *Nanoscale*, 2014, **6**, 3344–3352.
- 14 X. F. Xu, L. F. C. Pereira, Y. Wang, J. Wu, K. W. Zhang, X. M. Zhao, S. Bae, C. T. Bui, R. G. Xie, J. T. L. Thong, B. H. Hong, K. P. Loh, D. Donadio, B. W. Li and B. Ozyilmaz, *Nat. Commun.*, 2014, **5**, 3689.
- 15 S. S. Chen, Q. Z. Wu, C. Mishra, J. Y. Kang, H. J. Zhang, K. J. Cho, W. W. Cai, A. A. Balandin and R. S. Ruoff, *Nat. Mater.*, 2012, **11**, 203–207.
- 16 L. Zhu, G. Zhang and B. Li, *Phys. Rev. B: Condens. Matter*, 2014, **90**, 214302.
- 17 Z. Y. Ong, Y. Q. Cai, G. Zhang and Y. W. Zhang, *J. Phys. Chem. C*, 2014, **118**, 25272–25277.
- 18 A. Jain and A. J. H. McGaughey, *Sci. Rep.*, 2015, **5**, 8501.
- 19 G. Z. Qin, Q. B. Yan, Z. Z. Qin, S. Y. Yue, M. Hu and G. Su, *Phys. Chem. Chem. Phys.*, 2015, **17**, 4854–4858.
- 20 S. Plimpton, *J. Comput. Phys.*, 1995, **117**, 1–19.
- 21 J.-W. Jiang, T. Rabczuk and H. S. Park, *Nanoscale*, 2015, **7**, 6059–6068.
- 22 Z. Zhu and D. Tománek, *Phys. Rev. Lett.*, 2014, **112**, 176802.
- 23 J. Jin-Wu, *Nanotechnology*, 2015, **26**, 315706.
- 24 F. F. Abraham and I. P. Batra, *Surf. Sci.*, 1989, **209**, L125–L132.
- 25 L. D. Landau and E. M. Lifshitz, *Theory of Elasticity*, Pergamon, Oxford, 1995.
- 26 D. W. Brenner, O. A. Shenderova, J. A. Harrison, S. J. Stuart, B. Ni and S. B. Sinnott, *J. Phys.: Condens. Matter*, 2002, **14**, 783–802.
- 27 J. Tersoff, *Phys. Rev. Lett.*, 1988, **61**, 2879–2882.
- 28 B. W. Dodson, *Phys. Rev. B: Condens. Matter*, 1987, **35**, 2795–2798.
- 29 L. Lindsay, D. A. Broido and N. Mingo, *Phys. Rev. B: Condens. Matter*, 2010, **82**, 115427.
- 30 F. Müller-Plathe, *J. Chem. Phys.*, 1997, **106**, 6082–6085.
- 31 A. A. Balandin, S. Ghosh, W. Z. Bao, I. Calizo, D. Teweldebrhan, F. Miao and C. N. Lau, *Nano Lett.*, 2008, **8**, 902–907.
- 32 A. A. Balandin, *Nat. Mater.*, 2011, **10**, 569–581.
- 33 J. N. Hu, X. L. Ruan and Y. P. Chen, *Nano Lett.*, 2009, **9**, 2730–2735.
- 34 W. J. Evans, L. Hu and P. Keblinski, *Appl. Phys. Lett.*, 2010, **96**, 203112.
- 35 J. Zhang, X. Huang, Y. Yue, J. Wang and X. Wang, *Phys. Rev. B: Condens. Matter*, 2011, **84**, 235416.
- 36 J. Hu, S. Schiffl, A. Vallabhaneni, X. Ruan and Y. P. Chen, *Appl. Phys. Lett.*, 2010, **97**, 133107.
- 37 J. Hu, X. Ruan, Z. Jiang and Y. P. Chen, *AIP Conf. Proc.*, 2009, **1173**, 135–138.
- 38 J. W. Jiang, *Nanotechnology*, 2015, **26**, 055701.
- 39 J. W. Jiang and H. S. Park, *J. Phys. D: Appl. Phys.*, 2014, **47**, 385304.
- 40 R. Fei, A. Faghaninia, R. Soklaski, J.-A. Yan, C. Lo and L. Yang, *Nano Lett.*, 2014, **14**, 6393–6399.
- 41 J. Zhang, X. Wang and H. Xie, *Phys. Lett. A*, 2013, **377**, 721–726.
- 42 J. Zhang, X. Wang and H. Xie, *Phys. Lett. A*, 2013, **377**, 2970–2978.
- 43 J. Zhang and X. Wang, *Nanoscale*, 2013, **5**, 734–743.
- 44 H. Zhong and J. R. Lukes, *Phys. Rev. B: Condens. Matter*, 2006, **74**, 125403.
- 45 E. S. Landry and A. J. H. McGaughey, *Phys. Rev. B: Condens. Matter*, 2009, **80**, 165304.
- 46 J. Zhang, Y. Wang and X. Wang, *Nanoscale*, 2013, **5**, 11598–11603.
- 47 Y. Hong, L. Li, X. C. Zeng and J. Zhang, *Nanoscale*, 2015, **7**, 6286–6294.
- 48 A. A. Balandin, S. Ghosh, W. Bao, I. Calizo, D. Teweldebrhan, F. Miao and C. N. Lau, *Nano Lett.*, 2008, **8**, 902–907.
- 49 S. Ghosh, I. Calizo, D. Teweldebrhan, E. P. Pokatilov, D. L. Nika, A. A. Balandin, W. Bao, F. Miao and C. N. Lau, *Appl. Phys. Lett.*, 2008, **92**, 151911.
- 50 T. Y. Ng, J. J. Yeo and Z. S. Liu, *Carbon*, 2012, **50**, 4887–4893.
- 51 D. Liu, P. Yang, X. Yuan, J. Guo and N. Liao, *Phys. Lett. A*, 2015, **379**, 810–814.
- 52 G. Xu, C. M. Torres, J. Tang, J. Bai, E. B. Song, Y. Huang, X. Duan, Y. Zhang and K. L. Wang, *Nano Lett.*, 2011, **11**, 1082–1086.
- 53 J. Wurm, K. Richter and İ. Adagideli, *Phys. Rev. B: Condens. Matter*, 2011, **84**, 075468.
- 54 Y. Wang, B. Qiu and X. Ruan, *Appl. Phys. Lett.*, 2012, **101**, 013101.
- 55 P. K. Schelling, S. R. Phillpot and P. Keblinski, *Phys. Rev. B: Condens. Matter*, 2002, **65**, 144306.
- 56 D. P. Sellan, E. S. Landry, J. E. Turney, A. J. H. McGaughey and C. H. Amon, *Phys. Rev. B: Condens. Matter*, 2010, **81**, 214305.
- 57 M. M. Sadeghi, I. Jo and L. Shi, *Proc. Natl. Acad. Sci. U. S. A.*, 2013, **110**, 16321–16326.
- 58 A. S. Nissimagoudar and N. S. Sankeshwar, *Phys. Rev. B: Condens. Matter*, 2014, **89**, 235422.
- 59 B. Liu, J. A. Baimova, C. D. Reddy, S. V. Dmitriev, W. K. Law, X. Q. Feng and K. Zhou, *Carbon*, 2014, **79**, 236–244.
- 60 B. Liu, J. A. Baimova, C. D. Reddy, A. W.-K. Law, S. V. Dmitriev, H. Wu and K. Zhou, *ACS Appl. Mater. Interfaces*, 2014, **6**, 18180–18188.
- 61 J. Zhang, Y. Hong and Y. Yue, *J. Appl. Phys.*, 2015, **117**, 134307.

- 62 M. Li, J. Zhang, X. Hu and Y. Yue, *Appl. Phys. A*, 2015, **119**, 415–424.
- 63 P. G. Klemens, *J. Wide Bandgap Mater.*, 2000, **7**, 332–339.
- 64 P. G. Klemens, *Int. J. Thermophys.*, 2001, **22**, 265–275.
- 65 D. L. Nika, S. Ghosh, E. P. Pokatilov and A. A. Balandin, *Appl. Phys. Lett.*, 2009, **94**, 203103.
- 66 J. H. Seol, I. Jo, A. L. Moore, L. Lindsay, Z. H. Aitken, M. T. Pettes, X. Li, Z. Yao, R. Huang, D. Broido, N. Mingo, R. S. Ruoff and L. Shi, *Science*, 2010, **328**, 213–216.
- 67 L. Lindsay, D. A. Broido and N. Mingo, *Phys. Rev. B: Condens. Matter*, 2011, **83**, 235428.
- 68 T. Tritt, *Thermal conductivity: theory, properties, and applications*, Kluwer Academic/Plenum Publishers, 2004, pp. 114–115.